



PAPER

Design of tunable acoustic metamaterials through periodic arrays of resonant shunted piezos

To cite this article: L Airoldi and M Ruzzene 2011 *New J. Phys.* **13** 113010

View the [article online](#) for updates and enhancements.

You may also like

- [\(Invited\) Resonant Interlayer Tunneling in 2D Van Der Waals-Materials-Based Channel-Dielectric-Channel Systems and Possible Device and Circuit Applications](#)

Leonard F. Register, G. William Burg, Chris M Corbet et al.

- [Study on the Resonant Cavity for Low-level RF System at the PBP-CMU Electron Linac Laboratory](#)

W Foosang, N. Kangrang, S Pakluea et al.

- [A tunable planar inverted-F antenna with an RF MEMS switch for the correction of impedance mismatch due to human hand effects](#)

Yong-Hee Park, Jae-Hyoung Park, Yong-Dae Kim et al.

Design of tunable acoustic metamaterials through periodic arrays of resonant shunted piezos

L Airoidi¹ and M Ruzzene^{1,2,3}

¹ D Guggenheim School of Aerospace Engineering, Georgia Institute of Technology, Atlanta, GA 30332, USA

² G W Woodruff School of Mechanical Engineering, Georgia Institute of Technology, Atlanta, GA 30332, USA

E-mail: massimo.ruzzene@aerospace.gatech.edu

New Journal of Physics **13** (2011) 113010 (21pp)

Received 17 August 2011

Published 9 November 2011

Online at <http://www.njp.org/>

doi:10.1088/1367-2630/13/11/113010

Abstract. Periodic shunted piezoelectric patches are employed for the design of a tunable, one-dimensional metamaterial. The configuration considered encompasses a beam undergoing longitudinal and transverse motion, and a periodic array of piezoelectric patches with electrodes connected to a resonant electric circuit. The resulting acousto-electrical system is characterized by an internal resonant behavior that occurs at the tuning frequency of the shunting circuits, and is analogous in its operation to other internally resonating systems previously proposed, with the addition of its simple tunability. The performance of the beam is characterized through the application of the transfer matrix approach, which evaluates the occurrence of bandgaps at the tuning frequencies and estimates wave attenuation within such bands. Moreover, a homogenization study is conducted to illustrate the internal resonant characteristics of the system within an analytical framework. Experiments performed on the considered beam structure validate the theoretical predictions and illustrate its internal resonant characteristics and the formation of the related bandgaps.

³ Author to whom any correspondence should be addressed.

Contents

1. Introduction	2
2. Theoretical background	3
2.1. Configuration	3
2.2. Governing equations	4
3. Analysis of the dispersion properties	6
3.1. Transfer matrix	6
3.2. Beam configuration	7
3.3. Numerical results	7
4. Experimental results	8
4.1. The setup	9
4.2. Response in the space/time domain	10
4.3. Signal processing for the evaluation of dispersion	11
4.4. Wavenumber estimation from experimental measurements	14
5. Equivalent properties: a metamaterial perspective	16
5.1. Long-wavelength approximation	16
5.2. Equivalent mechanical properties	18
5.3. Dispersion relations	19
6. Conclusions	20
References	21

1. Introduction

Piezoelectric shunt damping is an attractive technique that offers a simple and potentially cost-effective solution for the attenuation of waves and vibrations in structures. The key element is a passive electrical network directly connected to the electrodes of the piezoelectric device mounted on the vibrating structure. In the configuration proposed by Hagood and von Flotow (1991), a resistive-inductive (RL) shunting circuit is shown to be equivalent to a tuned mechanical vibration absorber which can attenuate vibrations at frequencies in the vicinity of a selected mode of the structure. Subsequent studies have investigated complex shunting circuits capable of suppressing several structural modes through multiple resonating circuit branches or the implementation of negative impedance circuits (Forward 1979, Hollkamp 1994, Wu 1996, Preumont 1997, Behrens *et al* 2003). The approach proposed by Thorp *et al* (2001) involves a periodic array of RL-shunted piezos mounted on the structure as a way to create bandgaps centered at the tuning frequencies of the shunting circuits. The tunable characteristics of shunted piezo patches allow the equivalent mechanical impedance to be tuned so that bandgaps are generated over desired frequency ranges. Subsequently, the concept was applied to complex structures such as fluid-loaded axisymmetric shells (Thorp *et al* 2005) and plates (Spadoni *et al* 2009, Casadei *et al* 2010). These studies demonstrate how resonant piezoelectric shunts can be utilized to affect the equivalent mechanical properties of an elastic waveguide and therefore suggest their application for the development of metamaterials (Kushwaha *et al* 1993, Sigalas 1998, Martinsson and Movchan 2003, Sheng *et al* 2003, Huang *et al* 2009, Lu *et al* 2009). In fact, many proposed concepts for acoustic metamaterials consider configurations that derive their unique properties from resonators contained within each unit cell. Typical

designs feature inclusions with a phase velocity much lower than that of the matrix (Kushwaha and Djafari-Rouhani 1998). This allows production of attenuation bands at frequencies which are unrelated to scattering phenomena occurring at wavelengths of the order of the unit cell size (Bragg scattering), and are instead associated with a resonance within a unit cell. The opportunity is thus given to achieve low-frequency attenuation of waves, which has relevance, for example, for the control of vibrations and noise transmission. Different types of local resonators that have been proposed include the single degree of freedom mass-in-mass lattice systems (Lazarov and Jensen 2007, Yao *et al* 2008, Huang *et al* 2009), the multi-degrees of freedom resonators systems (presented in Huang and Sun 2010, Pai 2010, Sun *et al* 2010), coated cylinders/spheres oscillating in an epoxy matrix (Sheng *et al* 2007, Gao *et al* 2008) and Helmholtz resonators in parallel with an acoustic waveguide (Fang *et al* 2006, Cheng *et al* 2008).

In this paper, we illustrate how the periodic array of piezoelectric patches bonded to a one-dimensional (1D) waveguide previously investigated by Thorp *et al* (2001) can be interpreted as a 1D metamaterial with internally resonating units. Such units are characterized by the electrical resonances of the shunting circuits. Such resonant frequencies can be conveniently tuned through proper selection of the electrical impedance connected to each patch, so that no modification to the structure is necessary. Results are illustrated for a 1D waveguide consisting of a beam undergoing longitudinal and transverse motion, coupled to an array of shunted patches. The performance of the system in terms of dispersion characteristics, bandgaps and wave attenuation is predicted through the application of the transfer matrix (TM) method, and is subsequently verified experimentally. The experimental measurements are analyzed through proper signal processing techniques that also allow the accurate estimation of attenuation constants and dispersion in the neighborhood of the internal resonances, where the group velocity becomes negative. Analytical estimation of the equivalent properties of the system are also derived through a homogenization approach based on a long-wavelength approximation.

The paper is organized into six sections, including this introduction. Section 2 presents the theoretical background required for the analysis of the considered periodic system, while section 3 illustrates its dispersion characteristics. Section 4 presents the experimental procedures and results, and section 5 describes the developed homogenization approach for the estimation of the equivalent stiffness properties of the waveguide. Finally, section 6 summarizes the major findings of this paper and provides recommendations for future investigation.

2. Theoretical background

2.1. Configuration

We consider the dynamic behavior of the beam with a periodic array of shunted piezoelectric patches (figure 1(a)) obtained as the assembly of unit cells of the kind shown in figure 1(b). The beam behaves as a 1D waveguide that supports the propagation of axial and transverse waves. In the low-frequency range, the behavior of the waveguide can be conveniently described through the Euler–Bernoulli theory, applied to a beam with piecewise elastic and mass properties, as illustrated in the following section.

We refer to a coordinate system where ‘1’ and ‘3’, respectively, denote the axial and thickness directions. According to Hagood and von Flotow (1991), shunting of the piezoelectric patch with electrodes across the ‘3’ direction modifies Young’s modulus of the shunted patch

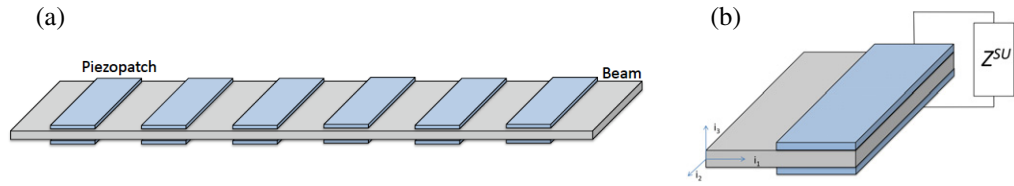


Figure 1. A periodic beam with an array of shunted piezo patches (a) and a unit cell with shunting through an electrical impedance Z^{SU} (b).

according to the following expression:

$$E_p^{\text{SU}}(\omega) = E_p^{\text{D}} \left(1 - \frac{k_{31}^2}{1 + i\omega C_p^\epsilon Z^{\text{SU}}(\omega)} \right), \quad (1)$$

where ω is the frequency, $i = \sqrt{-1}$, C_p^ϵ is the electrical capacitance of the piezo at constant strain, and $Z^{\text{SU}}(\omega)$ is the electrical impedance of the shunting circuit. Also in equation (1), k_{31} denotes the electro-mechanical coupling coefficient, and E_p^{D} is Young's modulus of the piezoelectric material when the shunting network is in an open-circuit configuration ($Z^{\text{SU}}(\omega) \rightarrow \infty$). This quantity is related to the piezo Young's modulus E_p through the expression $E_p^{\text{D}} = E_p / (1 - k_{31}^2)$ (Hagood and von Flotow 1991).

When a resistor-inductor shunt is applied to the piezoelectric material, $Z^{\text{SU}}(\omega) = R + i\omega L$, the piezo Young's modulus features a resonant behavior at a frequency ω_T that can be selected by tuning the inductor $L = 1/(\omega_T^2 C_p^\epsilon)$ (Hagood and von Flotow 1991, Hollkamp 1994, Wu 1996).

2.2. Governing equations

The longitudinal $u(x, t)$ and transverse $w(x, t)$ motion of the beam of figure 1 is described by the following set of partial differential equations:

$$\frac{\partial^2}{\partial x^2} \left[D(x) \frac{\partial^2}{\partial x^2} w(x, t) \right] + m(x) \frac{\partial^2}{\partial t^2} w(x, t) = 0, \quad (2)$$

$$\frac{\partial}{\partial x} \left[K(x) \frac{\partial}{\partial x} u(x, t) \right] - m(x) \frac{\partial^2}{\partial t^2} u(x, t) = 0, \quad (3)$$

where $D(x)$, $K(x)$, respectively, denote the bending and axial stiffness of the beam, while $m(x)$ is the mass per unit area. Given the beam configuration, a generic physical property of the beam $P(x)$ can be expressed as a piecewise function of period p , i.e.

$$P(x) = P(x + p), \quad (4)$$

which over a period centered at $x = 0$ can be expressed as

$$P(x) = \begin{cases} P_1 & -\alpha p < x < 0, \\ P_2 & 0 < x < (1 - \alpha)p, \end{cases} \quad (5)$$

with α denoting the ratio between the length of the interval with property P_1 and the length of the period p .

For the unit cell of figure 1, the linear mass of the beam is given by

$$m(x) = \begin{cases} \rho_b A_b, & -\alpha p < x < 0, \\ \rho_b A_b + 2\rho_p A_p, & 0 < x < (1 - \alpha)p, \end{cases} \quad (6)$$

while the axial and bending stiffnesses can, respectively, be expressed as

$$K(x) = \begin{cases} E_b A_b, & -\alpha p < x < 0, \\ E_b A_b + 2E_p^{\text{SU}}(\omega) A_p, & 0 < x < (1 - \alpha)p, \end{cases} \quad (7)$$

and

$$D(x) = \begin{cases} \frac{E_b b_b h_b^3}{12}, & -\alpha p < x < 0, \\ \frac{E_b b_b h_b^3}{12} + \frac{E_p^{\text{SU}}(\omega) b_p [(h + 2h_p)^3 - h^3]}{6}, & 0 < x < (1 - \alpha)p, \end{cases} \quad (8)$$

where ρ_b and E_b are the density and the Young's modulus of the beam material, h_b , b_b define the thickness and out-of-plane width of the base beam, and $A_b = b_b h_b$. Also, ρ_p is the density of the piezoelectric material, h_p , b_p denote the thickness and out-of-plane width of the piezo patch and $A_p = b_p h_p$.

For harmonic motion at frequency ω , equations (2) and (3) reduce to two ODEs in the spatial coordinate x , which can be combined in the following first-order system:

$$\mathbf{A}(x) \frac{d}{dx} \mathbf{z}(x) = \mathbf{B}(x) \mathbf{z}(x), \quad (9)$$

where the state vector \mathbf{z} contains displacement and stress resultants associated with axial and transverse motion, and it is defined as

$$\mathbf{z}(x) = [u, w, w_{,x}, N, M, Q]^T. \quad (10)$$

In equation (10), N , Q and M are the axial stress resultant, the shear force and the bending moment at location x . Also, in the equation above and in the remainder of the paper the notation capital boldface letters denote matrices, and lower case boldface letters are vectors. The matrices \mathbf{A} , \mathbf{B} in equation (9) are defined as

$$\mathbf{A}(x) = \text{diag}([K(x), 1, D(x), 1, -1, 1]) \quad (11)$$

and

$$\mathbf{B}(x) = \begin{bmatrix} 0 & 0 & 0 & 1 & 0 & 0 \\ 0 & 0 & 1 & 0 & 0 & 0 \\ 0 & 0 & 0 & 0 & 1 & 0 \\ -\omega^2 m(x) & 0 & 0 & 0 & 0 & 0 \\ 0 & 0 & 0 & 0 & 0 & 1 \\ 0 & -\omega^2 m(x) & 0 & 0 & 0 & 0 \end{bmatrix}. \quad (12)$$

Equation (9) can be rewritten as

$$\frac{d}{dx} \mathbf{z}(x) = \mathbf{C}(x) \mathbf{z}(x), \quad (13)$$

where $\mathbf{C} = \mathbf{A}^{-1} \mathbf{B}$ is a periodic matrix which varies in a piecewise fashion over the period p , i.e.

$$\mathbf{C}(x) = \begin{cases} \mathbf{C}_1, & -\alpha p < x < 0, \\ \mathbf{C}_2, & 0 < x < (1 - \alpha)p. \end{cases} \quad (14)$$

3. Analysis of the dispersion properties

3.1. Transfer matrix

Equation (13) describes a system of ODEs with periodic coefficients. According to the Floquet theorem, its solution can be expressed as

$$z(x + p) = \lambda z(x), \quad (15)$$

where $\lambda = e^{i\mu}$ is the Floquet multiplier, with $\mu = kp$ denoting the propagation constant and k the wavenumber. The Floquet multipliers are obtained by relating the solution of equation (13) at a location $x + p$ and x through a TM T :

$$z(x + p) = Tz(x). \quad (16)$$

For the case at hand, the formulation of the TM exploits the piecewise nature of the periodicity, which allows close form expressions. With reference to a unit cell, equation (16) can be expressed as

$$z[(1 - \alpha)p] = Tz(-\alpha p), \quad (17)$$

where T is given by

$$T = T_2 T_1. \quad (18)$$

In the equation above, the matrix T_1 relates the state vectors at $x = -\alpha p$ to the state vector at $x = 0$, while the matrix T_2 relates the state vectors at $x = 0$ and at $x = (1 - \alpha)p$. Matrices T_1 and T_2 can be formulated from the analytical solution of the governing equation over the first and second portions of the unit cell, i.e.

$$\frac{d}{dx}z(x) = C_1 z(x), \quad x \in [-\alpha p, 0] \quad (19)$$

and

$$\frac{d}{dx}z(x) = C_2 z(x), \quad x \in [0, (1 - \alpha)p], \quad (20)$$

which give

$$z(0) = e^{\alpha p C_1} z(-\alpha p), \quad x \in [-\alpha p, 0], \quad (21)$$

$$z[(1 - \alpha)p] = T_2 z(0), \quad x \in [0, (1 - \alpha)p]. \quad (22)$$

Therefore

$$T_1 = e^{\alpha p C_1} \quad (23)$$

and

$$T_2 = e^{(1-\alpha)p C_2}. \quad (24)$$

Continuity of displacements and stresses at the interface of the two portions of the materials leads to

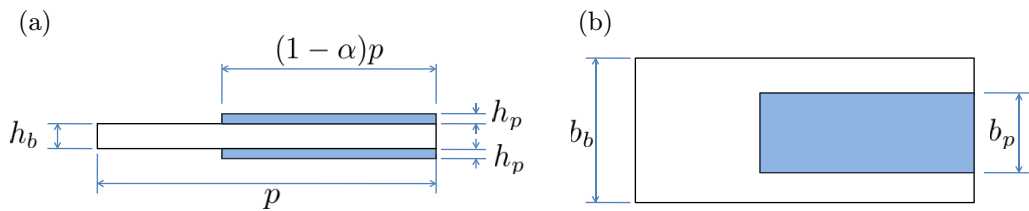
$$z[(1 - \alpha)p] = e^{(1-\alpha)p C_2} e^{\alpha p C_1} z(-\alpha p) = T_2 T_1 z(-\alpha p) = Tz(-\alpha p). \quad (25)$$

Table 1. Unit cell geometry.

p (mm)	α	h_b (mm)	b_b (mm)	h_p (mm)	b_p (mm)
54	0.35	3.5	32	0.8	18

Table 2. Properties of piezoelectric material.

E_p (GPa)	ρ_p (kg m^{-3})	k_{31}	$\varepsilon_{33}^s/\varepsilon_0$	ε_0 (pF m^{-1})	C_p^ε (nF)
63	7800	0.35	2500	8.854	15

**Figure 2.** Sketch of the unit cell for the beam. (a) Side view. (b) Top view.

3.2. Beam configuration

The periodic beam is formed by the assembly of unit cells shown in figure 2. The geometrical parameters of the unit cell are summarized in table 1. The beam is made of aluminum (Young's modulus $E_b = 69$ GPa and density $\rho_b = 2700$ kg m^{-3}), while the piezoelectric patch has the properties listed in table 2.

3.3. Numerical results

The dispersion relations associated with the longitudinal and transverse motion of the beam are evaluated through the TM approach. The results for two different tuning frequencies are reported here. The internal resonance of the circuit is selected at 5000 and 11 000 Hz. Such tuning frequencies are obtained with inductance values for the shunting circuit, respectively, equal to $L = 33.4$ mH and $L = 6.7$ mH. The results for different values of shunting resistance are also reported. Figure 3 presents the dispersion relations for the said beam when the electric circuit resonates at 5000 Hz (blue lines) and at 11 000 Hz (red line) for shunting resistances of 25 and 50 Ω . Specifically, figure 3(a) presents the branch associated with longitudinal motion, while figure 3(b) shows the results for the transverse mode. The two modes can be studied separately as completely decoupled by the beam model employed for the analysis. Both plots feature the expected resonant behavior at the resonant (tuning) frequency of the shunting circuit, which also defines the center of an attenuation band. Such an attenuation band is identified by nonzero values of the imaginary part of the wavenumber, which characterizes the conditions of propagation with attenuation. Of note is the fact that the resistive component in the shunting LR circuit acts as a dissipation term, which has the effect of affecting the resonant behavior of the circuit. Low dissipation with low resistance leads to a sharp resonant peak, and a

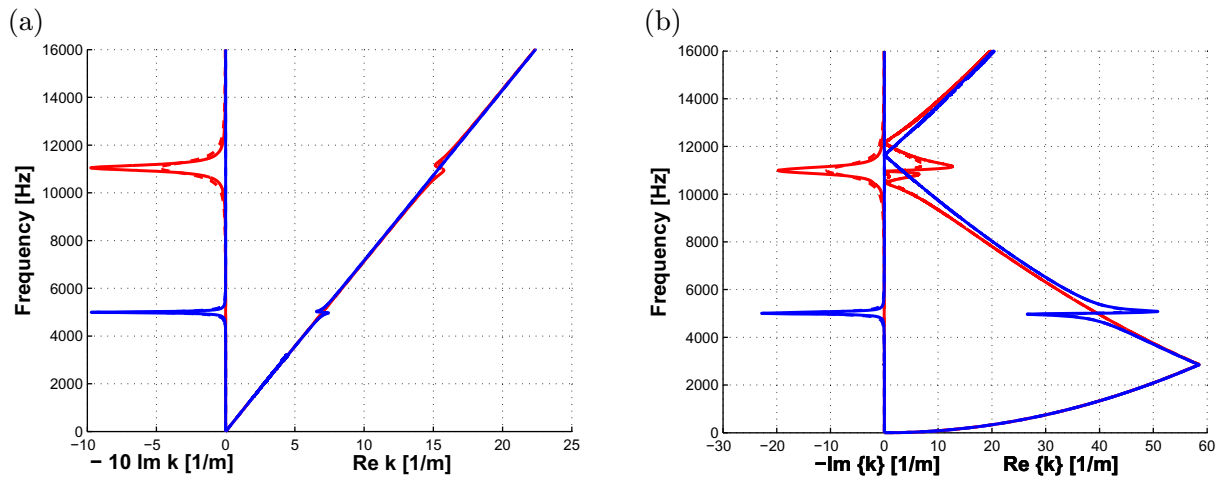


Figure 3. Real and imaginary parts of the wavenumber for axial (a) and bending (b) modes for different tunings of the piezo shunts ($f_T = 5$ kHz—blue line, $f_T = 11$ kHz—red line; $R = 25 \Omega$ —solid lines, $R = 50 \Omega$ —dashed lines). (a) Longitudinal motion. (b) Bending motion.

correspondingly large attenuation, which, however, occurs over a narrower frequency band. In contrast, high resistance values lead to a smoother resonant behavior, with lower attenuation occurring over a broader frequency band. Hence, if the objective is the achievement of high attenuation over a frequency band which is as large as possible, a compromise in terms of resistance must be struck between bandwidth and attenuation, as defined by the magnitude of the imaginary part of the wavenumber (Spadoni *et al* 2009).

Additional analysis of the dispersion branches for axial and transverse motion reveals some interesting features. As expected, the wavenumber range identified by the TM analysis is different for the two branches, and for the transverse mode it reaches the boundary of the first Brillouin zone, which is located at $k = \pi/p \approx 58.2 \text{ m}^{-1}$. At this value, the branch appears as folding back, which is the result of the periodicity of the domain and the dual periodicity in physical and wavenumber space (figure 3(b)). The wavenumber range for the axial mode does not reach such a bound in the considered frequency range, and therefore no branch folding is observed (figure 3(a)). Branch folding is a feature that is characteristic of all periodic domains, so that their dispersion properties can be characterized solely through the analysis of the first Brillouin zone. In general, however, and specifically when experimental studies are conducted, it is important to keep track of the entire frequency/wavenumber spectrum, since the branches beyond the first Brillouin zone may be measured and/or need to be properly tracked. In fact, the spatial resolution of the measurements typically goes beyond the spatial sampling corresponding to the limit of the first Brillouin zone, so that shorter wavelengths and correspondingly higher frequencies can be detected. This discussion is of particular relevance in light of the experimental results presented in the following sections.

4. Experimental results

Experimental investigations are performed on a beam with a periodic array of piezoelectric patches. The beam is excited by a piezo patch, which induces a transient wave propagating

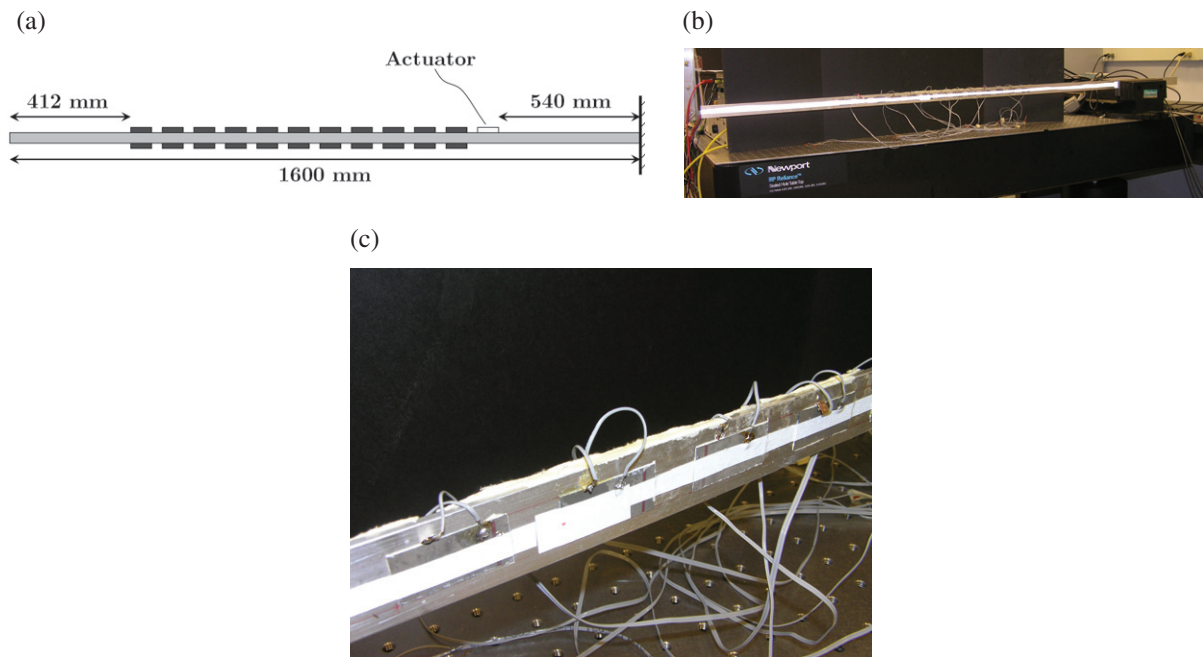


Figure 4. Sketch (a) and picture (b) of the experimental cantilever beam. A detail (c) illustrates the connection between piezo electrodes and electric circuits.

along the beam. The motion of the beam is recorded by a scanning laser Doppler vibrometer (SLDV). The SLDV records the velocity of a moving surface over a refined grid of measurement points. It exploits the Doppler effect on an incident laser beam, through which the component of motion of the surface parallel to the laser beam is recorded. The spatial refinement obtained through the SLDV's scanning mechanisms allows the detailed characterization of the recorded wavefield. Specifically, the recorded data have fine temporal and spatial resolutions sufficient for the estimation of the frequency/wavenumber content of the beam response, and the evaluation of the dispersion properties of the beam. This is performed through the application of 1D and 2D FT of the recorded data. Tests are conducted for various tunings of the shunting circuits to illustrate the occurrence of attenuation bands over selected frequency ranges.

The use of an SLDV as a sensor limits the investigations to the transverse motion of the beam, since the sensitivity of the laser allows only the detection of the component of motion perpendicular to the laser beam, which is normally incident to the beam surface.

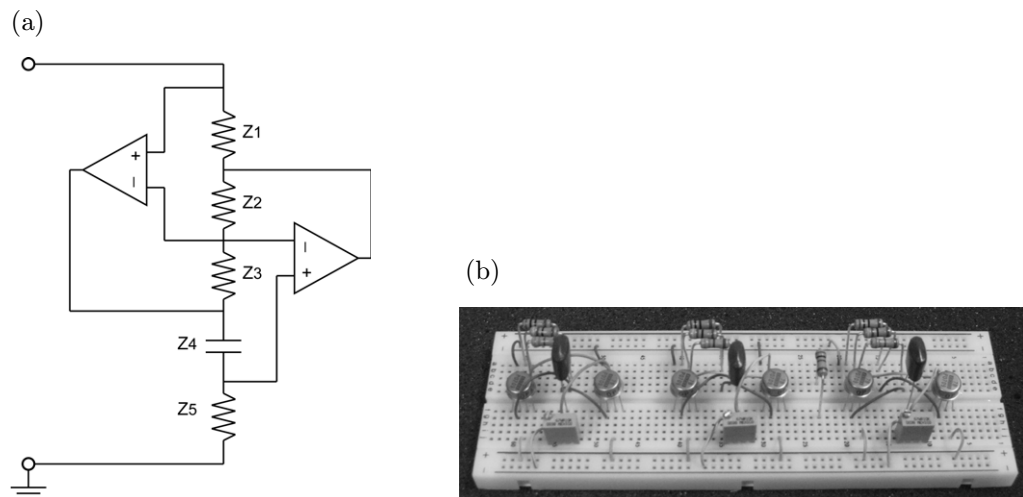
4.1. The setup

Tests were conducted on the beam shown in figure 4. The beam is made of aluminum, is 1.6 m long and features an array of 11 piezoelectric patches equally spaced over a portion of the length. The unit cell configuration replicates the schematic of figure 2 and has the dimensions listed in table 1.

The resonant shunted circuits are implemented through the application of a synthetic inductor (Antoniou's circuit) because of the high value of inductance needed for the desired frequency tunings and for the flexibility in the circuit tuning procedure; see figure 5 (Riordan 1967, Casadei *et al* 2010).

Table 3. Tuning settings for the experimental circuit (nominal values).

f_T (Hz)	Z_1 (Ω)	Z_2 (Ω)	Z_3 (Ω)	Z_4 (nF)	Z_5 (Ω)	R (Ω)
5000	3300	2200	100	100	2229	33
11 000	680	1000	100	100	988	47

**Figure 5.** Experimental resonant circuit. (a) Sketch of Antoniou circuit. (b) Picture of three resonant circuits.

In the configuration tested, each pair of co-located piezoelectric patches is connected in series to a resonant shunting circuit (figure 4(c)). The electric networks were tuned at the frequencies of 5000 and 11 000 Hz. The nominal values of the electric components Z_i required for these tunings are reported in table 3.

The beam is excited by the piezo actuator shown in figure 4, which is fed a pulse signal of $40 \mu\text{s}$ duration and 50 V amplitude. The time duration is selected for broadband excitation of the beam motion. The velocity of the beam is measured in 645 equally spaced points over the entire length by the SLDV (Polytec model PSV-400M2). At each measurement point x_i ($i = 1, \dots, 645$), the recorded time record contains 1024 samples, acquired at a sampling frequency of 256 kHz. Measurement noise is reduced through a low-pass digital filtering at 16 kHz, and by taking ten averages at each point with a repetition rate of 10 Hz.

4.2. Response in the space/time domain

The result of each experiment is the beam response, which is stored in a 2D array $w(x, t)$ that contains the time variation of the transverse velocity of the beam at location x . Figure 6(a) shows an example recorded when all shunts are connected to open circuits. This represents a baseline configuration against which the performance of various shunted strategies can be compared. The space/time response clearly shows the propagation of two waves, which emanate from the excitation location at approximately $x = 1$ m and subsequently reach the ends of the beam where they are reflected. The recorded wavefield appears, as expected, highly dispersive, as the

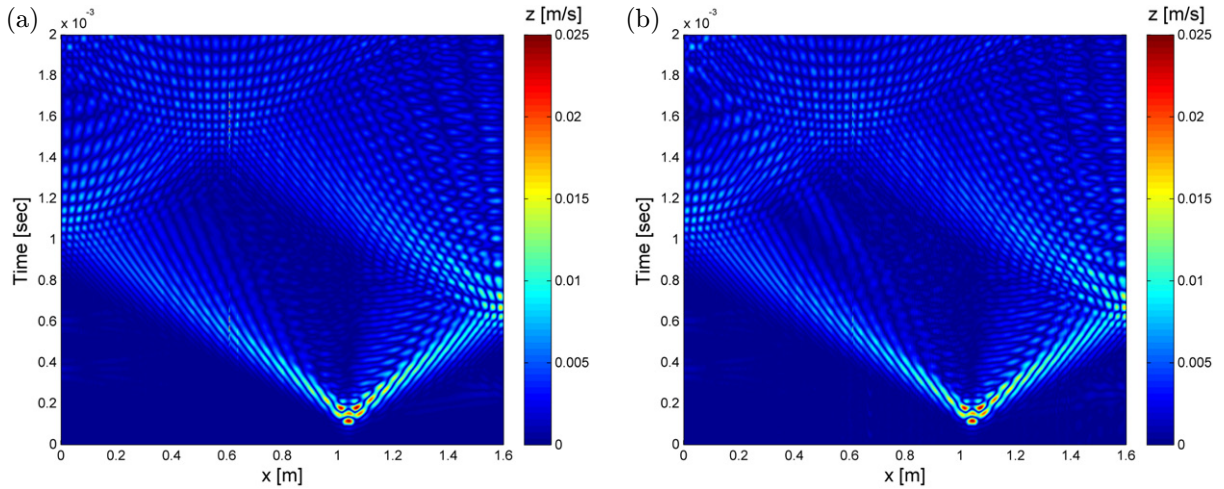


Figure 6. Experimental space/time response $w(x, t)$ of the beam in the space–time domain, tuning at 5000 Hz and $R = 33 \Omega$. (a) Open circuit. (b) Closed circuit.

applied pulse becomes increasingly distorted as it propagates along the length of the beam. The space/time response recorded with the shunts tuned at 5000 Hz and with a resistance value of $R = 33 \Omega$ displayed in figure 6(b) shows a similar behavior. Careful observation of the plot, however, unveils slightly stronger dispersion in comparison to the case with the open shunts. The evaluation of the effects of the shunts on wave propagation requires further analysis, which leads to the estimation of the dispersion relations for the beam from the recorded response.

4.3. Signal processing for the evaluation of dispersion

The estimation of the dispersion properties for the beam is performed by transforming the recorded response $w(x, t)$ into the frequency/wavenumber through a 2DFT:

$$W(k, \omega) = \int_{-\infty}^{+\infty} \int_{-\infty}^{+\infty} w(x, t) e^{-i(kx + \omega t)} dt dx. \quad (26)$$

This operation, which can be simply performed through built-in FFT routines, does however require preliminary post-processing of the data in order to obtain clear dispersion representations. First, only the left-propagating wave is analyzed by windowing the response in space in the $x \in [0, 1]$ m interval. Time windowing is also performed for $t = [0, 1.2]$ msec. The next important step consists in the removal of the boundary reflections. Reflections lead to the occurrence of dominant harmonic terms, which correspond to the resonant frequencies of the beam and their associated wavenumber. The presence of such harmonic terms causes the frequency/wavenumber domain representation to be discontinuous, with energies concentrated at the frequency/wavenumber values corresponding to the frequency and wavenumber of the resonant modes. As the objective here is to determine the occurrence of attenuation zones in the frequency/wavenumber relations, a discontinuous frequency/wavenumber spectrum would make the identification of such zones difficult and possibly ambiguous. Removal of the boundary reflection simulates the response of an infinite domain, which is characterized by

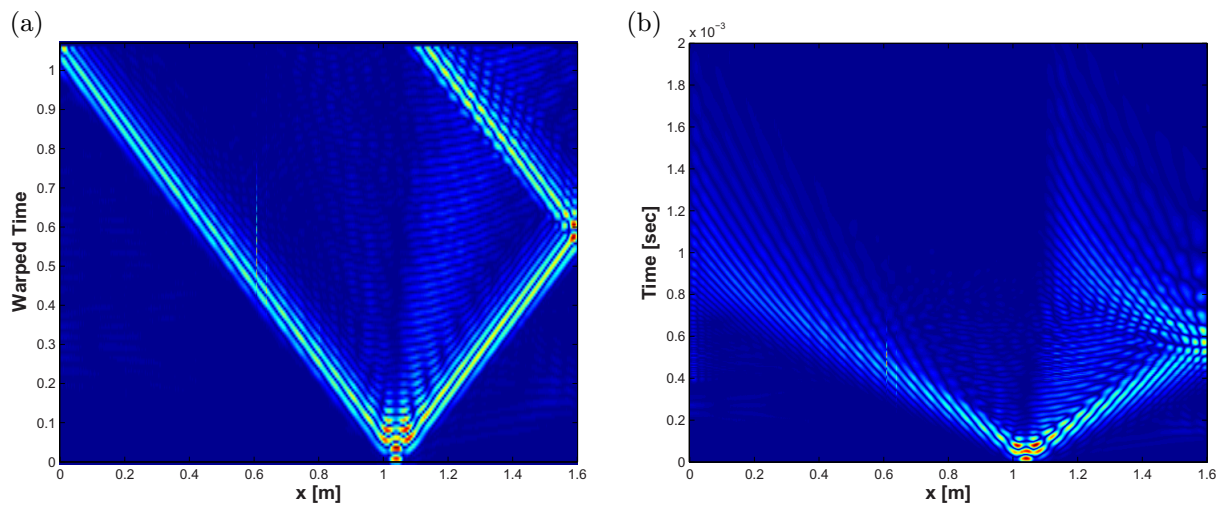


Figure 7. Warped and unwarped responses upon removal of the reflection at the left boundary. (a) Warped. (b) Unwarped.

continuous dispersion characteristics, where the presence of a frequency gap corresponding to an attenuation zone can be immediately identified.

The removal of the reflection from the boundary can be performed through proper time windowing of the signal, but is significantly complicated by the dispersive nature of the wave. In order to properly identify and then eliminate the reflection from the left boundary, dispersion is compensated here through transformation into the space-warped time domain by applying the warped frequency transform (WFT) proposed by De Marchi *et al* (2008). The WFT is a linear transformation, which is based on the *warping* of the frequency domain according to the dispersion properties of the medium of interest. This allows the representation of the signal in the warped-time axis where it appears non-dispersive. The result of this operation is illustrated in figure 7(a), where the warped-time axis is limited to the range preceding the left boundary reflection through proper windowing. The application of the inverse WFT returns the signal to the space/time domain where the boundary reflection from the left appears as completely removed (see figure 7(b)).

The windowed response is finally analyzed through a 2DFT, whose amplitude $|W(k, \omega)|$ can be represented as a surface in the frequency/wavenumber domain. The contour plot of the 2DFT surface for a beam with open circuits is shown in figure 8(a), which shows how the maxima of the contour plots outline the dispersion relation for the beam. The plot also shows that the beam is excited in a frequency range spanning approximately an interval from 3000 Hz up to the selected cut-off frequency of 16 000 Hz. Within this range, a continuous frequency/wavenumber relation can be observed. The results for shunts tuned at 5000 Hz presented in figure 8(b) clearly show the presence of a gap in the frequency/wavenumber spectrum at the tuning frequency.

These experimental results can be used for the analysis and validation of the numerical predictions obtained through the TM approach. The dispersion relations computed numerically can in fact be overlapped to the experimental frequency/wavenumber contours for a direct comparison. The results are presented in figure 9, where plots for the two tunings considered are presented. Numerical results presented as red lines extend to a wavenumber range that

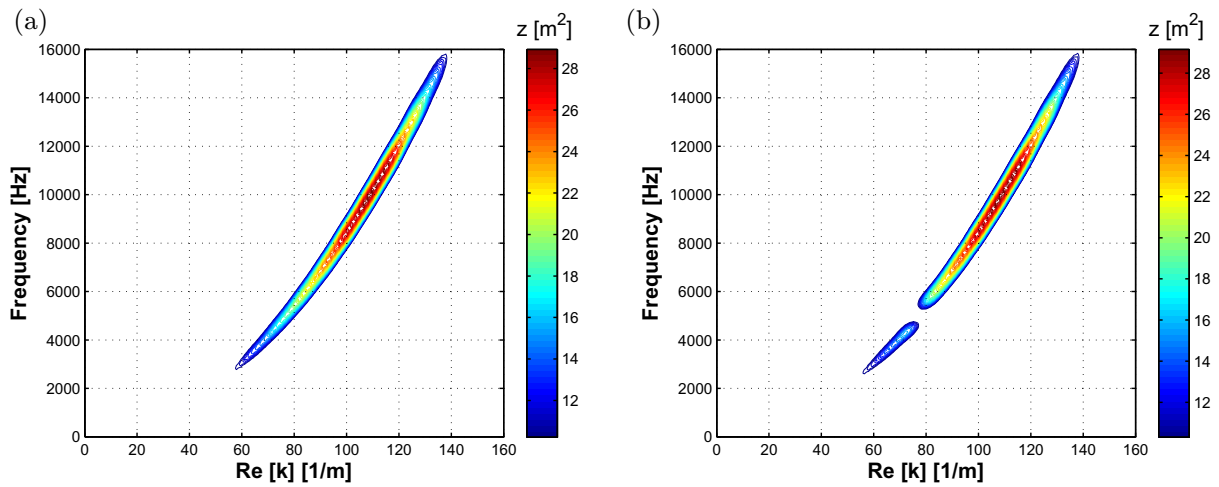


Figure 8. Contour of the amplitude of the 2DFT $|W(k, x)|$ outlining the dispersion properties for the beam with open shunts and with shunts tuned at 5000 Hz and $R = 33 \Omega$. (a) Open shunts. (b) Shunts tuned at 5000 Hz and $R = 33 \Omega$.

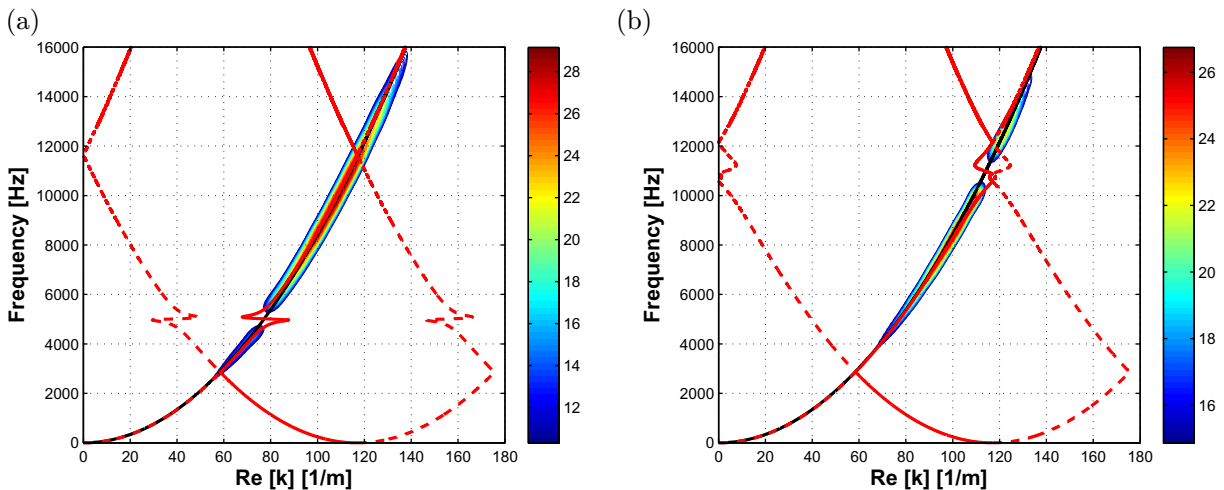


Figure 9. Comparison of the dispersion relations of the experimental beam and numerical results obtained with the TM formulation (red lines). The black solid line corresponds to the analytical dispersion relation for a homogeneous beam, with no periodic array of patches. (a) Tuning at 5000 Hz and $R = 33 \Omega$. (b) Tuning at 11000 Hz and $R = 47 \Omega$.

exceeds the bounds of the first Brillouin zone, in order to match the range of the experimental results. Several branches need to be included in order to follow the experimental observations, which, however, are very well predicted by the numerical predictions. Of note is the fact that the resonant properties of the beam predicted by the TM correspond to the frequency gap observed experimentally at the tuning frequency. For comparison purposes, it is also interesting to plot the dispersion branch for transverse wave in a homogeneous beam, presented here as a black solid line. This dispersion branch follows very well the maximum ridge of the contour,

which suggests that in the absence of shunting effects, and away from the tuning frequency, the beam essentially behaves as a homogeneous, non-periodic medium. Only the presence of the resonant piezos tuned at the selected frequencies affects the wave propagation properties of the waveguide. In essence, the physical periodicity introduced by the periodic placement of the piezos along the beam and the periodic modulation in the mechanical impedance due to the added mass and stiffness of the bonded piezos is not sufficient to create any attenuation zone through Bragg scattering, although the considered wavenumber range far exceeds the limit of the first Brillouin zone. This behavior partially justifies the use of a long wavelength approximation for the development of equivalent properties of the shunted waveguide as attempted in the next section.

4.4. Wavenumber estimation from experimental measurements

The spatial resolution provided by the considered experimental setup allows the quantitative estimation of the wavenumbers from experimental data. Both real and imaginary parts of the wavenumber can be estimated as a function of frequency, so that attenuation frequency bands can be quantified. The approach is based on the estimation of the spatial variation of the Fourier transform of the response evaluated at each frequency of interest. The procedure can be outlined by considering the measured response as the superposition of harmonic waves of the kind:

$$w(x, t) \approx \sum \hat{w}_i(x, t), \quad (27)$$

where

$$\hat{w}(x, t)_i = \hat{w}_0(\omega_i) e^{i[k(\omega_i)x - \omega_i t]} \quad (28)$$

is the i th harmonic component, where $k = k(\omega)$ due to the dispersive nature of the medium. The Fourier transform of $\hat{w}(x, t)_i$ at ω_i is evaluated as follows:

$$W(x, \omega) = \int_{-\infty}^{+\infty} \hat{w}(x, t)_i e^{-i\omega t} dt, \quad (29)$$

which evaluated at $\omega = \omega_i$ is given approximately by

$$W(x, \omega_i) \approx \hat{w}_0(\omega_i) e^{ik_i x}, \quad (30)$$

where $k_i = k(\omega_i)$. The wavenumber $k_i = k_{iR} + ik_{iI}$ is generally a complex number, so that equation (30) can be rewritten as

$$\hat{W}_i(x, \omega_i) \approx \hat{w}_0(\omega_i) e^{-k_{iI} x} e^{ik_{iR} x}. \quad (31)$$

Analysis of equation (31) reveals that the estimation of the FT of the recorded data and the evaluation of the variation of the resulting expression along the spatial coordinate x allow for the estimation of the spatial decay of the response amplitude and the phase evolution in space at a given frequency. This in turn leads to estimation of the attenuation constant as defined by the imaginary component of the wavenumber k_{iI} , and of its real component, which are, respectively, given by

$$k_{iI}(x_f - x_i) = \log[|W(x, \omega_i)|] \quad (32)$$

and

$$k_{iR}(x_f - x_i) = \arg[W(x, \omega_i)], \quad (33)$$

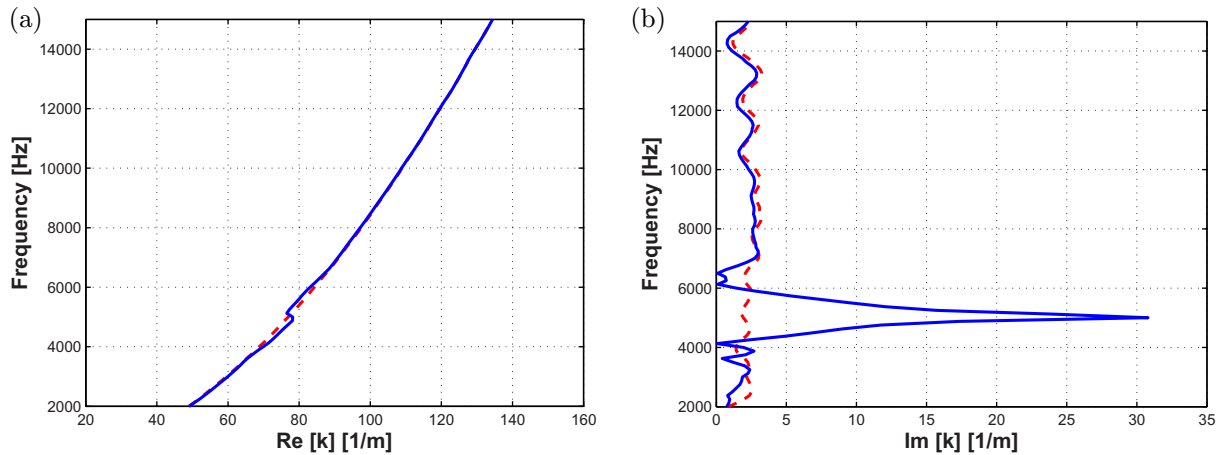


Figure 10. Experimentally estimated wavenumbers: open circuit (red dashed line), shunted circuits with tuning at 5000 Hz and resistor $R = 33 \Omega$ (blue solid line).

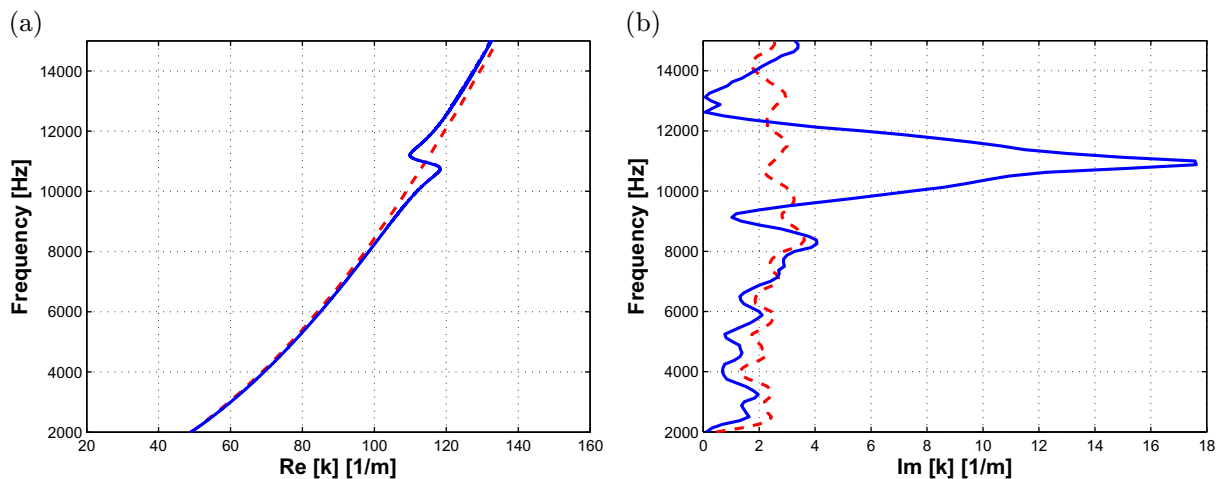


Figure 11. Experimentally estimated wavenumbers: open circuit (red dashed line), shunted circuits with tuning at 11 000 Hz and resistor $R = 47 \Omega$ (blue solid line).

where $x \in [x_i, x_f]$, with x_i, x_f denoting the initial coordinate and final coordinate over which the spatial decay and phase linear modulation are interpolated. Application of equations (32) and (33) to the experimental results allows the quantification of the wavenumber variation over the frequency range of interest and particularly the evaluation of the attenuation constant, which was not possible through the application of the 2DFT illustrated previously.

Examples of the estimated wavenumber components (real and imaginary parts) are presented in figures 10 and 11, where the red dashed lines correspond to the case of open circuits, while the solid blue lines are the results for shunting at the tuning frequencies considered. Both results clearly illustrate how shunting of the circuits at a given frequency creates an attenuation frequency band centered at the tuning frequency. Such a band is defined by large nonzero values of the imaginary part of the wavenumber, also known as the attenuation constant. In the same

frequency range, the real part of the wavenumber defining the propagation component undergoes a resonant behavior, which is consistent with that predicted numerically (see figure 9). The behavior of the dispersion properties around the frequency of internal resonance is typical of periodic systems with internal resonating properties as discussed in the introduction to this paper. Of note is the fact that the case of open circuits does not lead to an absolute zero for the attenuation constant, which may be affected by other sources of dissipation, which are inevitably present in an experimental setup.

5. Equivalent properties: a metamaterial perspective

The analysis presented in the previous sections can be further elaborated by seeking analytical expressions which provide insight into the behavior of the system when undergoing internal resonance through the shunting circuits. The investigations developed herein aim at developing equivalent models for the considered class of waveguides, which include the effects of the shunting circuit as part of a set of equivalent mechanical properties.

The theory is developed for the case of the beam undergoing axial and transverse motion. The results of the study are compared with the experimental measurements recorded for the beam in bending. The developments require the assumption that the scale of periodicity is much smaller than the wavelength considered. An interesting behavior is, however, observed, whereby good agreement between the predictions of the equivalent model and experiments is found in spite of the fact that the wavelengths corresponding to the frequency tunings are beyond the first Brillouin zone. This confirms that the periodicity introduced by the spacing of the piezoelectric patches does not affect the dynamic behavior of the system and therefore that the beam in the absence of shunting behaves as a homogeneous, non-periodic system. Based on this observation, one can interpret the considered system as the embodiment of a *metamaterial* concept, whereby unusual wave mechanics is achieved in the considered waveguide through the coupling between the primary structure and a resonating secondary system.

5.1. Long-wavelength approximation

The general formulation of equation (13) provides the basis for the analytical evaluation of the effects of the shunting circuit parameters on the wave characteristics of the considered waveguide. The study evaluates the resonant characteristics of the shunting circuit and their effect on the equivalent mechanical properties of the beam. Such behavior can be analytically investigated in the long wavelength limit or $k \rightarrow 0$. For $k \rightarrow 0$, it is convenient to introduce two scales to describe the problem, as is customary in homogenization problems for systems with periodically varying properties (Oleinik 1985, Hassani 1998, Ni and Cheng 2005). A second scale $y = x/\epsilon$ describes the periodicity of the domain, in addition to the large-scale coordinate x which governs the long-wavelength behavior of the system. Assuming that $\epsilon \ll 1$, so that $y \ll x$, leads to a two-scale expansion. Accordingly, equation (13) is expressed as

$$\frac{d}{dx}z(x, y) = C(x, y)z(x, y). \quad (34)$$

In the long wavelength, however, the properties of the beam can be considered as homogenous and therefore

$$C(x, y) = C(x, x/\epsilon) \approx C(y). \quad (35)$$

Next, the state vector is expanded according to the two-scale expansion

$$\mathbf{z}(x) = \mathbf{z}^{(0)}(x, y) + \epsilon \mathbf{z}^{(1)}(x, y) + \epsilon^2 \mathbf{z}^{(2)}(x, y) + \dots \quad (36)$$

and the spatial derivative in equation (34) is rewritten as

$$\frac{d}{dx} = \frac{\partial}{\partial x} + \frac{1}{\epsilon} \frac{\partial}{\partial y}. \quad (37)$$

Substituting equations (36) and (37) in equation (34) gives

$$\frac{\partial}{\partial x} \mathbf{z}^{(0)} + \frac{1}{\epsilon} \frac{\partial}{\partial y} \mathbf{z}^{(0)} + \epsilon \frac{\partial}{\partial x} \mathbf{z}^{(1)} + \frac{\partial}{\partial y} \mathbf{z}^{(1)} + \dots = \mathbf{C}(y)(\mathbf{z}^{(0)} + \epsilon \mathbf{z}^{(1)} + \dots), \quad (38)$$

which leads to the following set of ordered equations:

$$\epsilon^{-1} : \frac{\partial}{\partial y} \mathbf{z}^{(0)} = 0, \quad (39)$$

$$\epsilon^0 : \frac{\partial}{\partial x} \mathbf{z}^{(0)} + \frac{\partial}{\partial y} \mathbf{z}^{(1)} = \mathbf{C}(y) \mathbf{z}^{(0)}, \quad (40)$$

$$\epsilon^1 : \frac{\partial}{\partial x} \mathbf{z}^{(1)} = \mathbf{C}(y) \mathbf{z}^{(1)}. \quad (41)$$

Equation (39) implies that

$$\mathbf{z}^{(0)}(x, y) = \mathbf{z}^{(0)}(x), \quad (42)$$

while equation (40) can be simplified by integrating both sides over a period p , which gives

$$p \frac{\partial}{\partial x} \mathbf{z}^{(0)}(x) = \int_{-\alpha p}^{(1-\alpha)p} \mathbf{C}(y) dy \mathbf{z}^{(0)}(x). \quad (43)$$

The result from equation (42) can be exploited along with the well-known fact that the integral of the derivative of a periodic function over its period is equal to zero, i.e.

$$\int_{-\alpha p}^{(1-\alpha)p} \frac{\partial}{\partial y} \mathbf{z}^{(1)} dy = 0. \quad (44)$$

Equation (43) can be rewritten as

$$\frac{d}{dx} \mathbf{z}^{(0)}(x) = \mathbf{C}_{\text{eq}} \mathbf{z}^{(0)}(x), \quad (45)$$

which represents the governing equation for a beam of the kind considered whose equivalent homogeneous properties are given by

$$\mathbf{C}_{\text{eq}} = \frac{1}{p} \int_{-\alpha p}^{(1-\alpha)p} \mathbf{C}(y) dy. \quad (46)$$

Given the step-wise nature of the considered configuration, \mathbf{C}_{eq} is given by

$$\mathbf{C}_{\text{eq}} = \alpha \mathbf{C}_1 + (1 - \alpha) \mathbf{C}_2. \quad (47)$$

5.2. Equivalent mechanical properties

For the waveguide under study, the extended expression for \mathbf{C}_{eq} is

$$\mathbf{C}_{\text{eq}} = \begin{bmatrix} 0 & 0 & 0 & \frac{1}{K_{\text{eq}}} & 0 & 0 \\ 0 & 0 & 1 & 0 & 0 & 0 \\ 0 & 0 & 0 & 0 & \frac{1}{D_{\text{eq}}} & 0 \\ -\omega^2 m_{\text{eq}} & 0 & 0 & 0 & 0 & 0 \\ 0 & 0 & 0 & 0 & 0 & -1 \\ 0 & -\omega^2 m_{\text{eq}} & 0 & 0 & 0 & 0 \end{bmatrix}, \quad (48)$$

where m_{eq} , K_{eq} and D_{eq} are the equivalent linear mass, axial and bending stiffnesses of the beam, which are, respectively, given by

$$m_{\text{eq}} = \alpha m_1 + (1 - \alpha)m_2, \quad (49)$$

$$K_{\text{eq}} = \frac{K_1 K_2}{\alpha K_1 + (1 - \alpha)K_2}, \quad (50)$$

$$D_{\text{eq}} = \frac{D_1 D_2}{\alpha D_1 + (1 - \alpha)D_2}, \quad (51)$$

where m_i , K_i and D_i with $i = 1, 2$ denote the linear mass, axial and bending stiffnesses in each interval of the unit cell.

It is interesting to note how the results obtained within the considered long-wavelength approximation correspond to the well-known relations obtained through the application of the rule of mixture for composite materials. Of note is the fact that the variability of the piezoelectric elastic modulus, equation (1), leads to a frequency-dependent axial stiffness $K_2(\omega)$ and in turn to an equivalent stiffness $K_{\text{eq}}(\omega)$, which is also frequency dependent. Given the expressions for the elastic modulus of the shunted piezo patch (equation (1)), $K_{\text{eq}}(\omega)$ is given by

$$K_{\text{eq}}(\omega) = \frac{E_b A_b [(1 + \bar{g}) (1 + \omega^2 L C_p^\varepsilon + i\omega R C_p^\varepsilon) - \bar{g} k_{31}^2]}{[\alpha + (1 - \alpha) (1 + \bar{g})] (1 + \omega^2 L C_p^\varepsilon + i\omega R C_p^\varepsilon) - (1 - \alpha) \bar{g} k_{31}^2}, \quad (52)$$

where $g E_b A_b = E_p^{\text{SU}} A_p$ and $\bar{g} = g/(1 - k_{31}^2)$.

Similarly, the equivalent bending stiffness for the beam is given by

$$D_{\text{eq}}(\omega) = \frac{E_b I_b [(1 + \bar{\gamma}) (1 + \omega^2 L C_p^\varepsilon + i\omega R C_p^\varepsilon) - \bar{\gamma} k_{31}^2]}{[\alpha + (1 - \alpha) (1 + \bar{\gamma})] (1 + \omega^2 L C_p^\varepsilon + i\omega R C_p^\varepsilon) - (1 - \alpha) \bar{\gamma} k_{31}^2}, \quad (53)$$

where $I_b = \frac{1}{12} b_b h_b^3$, $I_p = \frac{1}{12} b_p [2(\frac{1}{2} h_b + h_p)^3 - h_b^3]$, $\gamma E_b I_b = E_p^{\text{SU}} I_p$ and $\bar{\gamma} = \gamma/(1 - k_{31}^2)$.

Frequency variations of equivalent bending and axial stiffnesses are presented in figure 12 for different tunings of the shunt circuits. The resonant behavior of the shunts is reflected in the equivalent mechanical behavior of the waveguide, which is a behavior observed for other internally resonating metamaterials and has been interpreted as the result of an apparent negative stiffness at the internal resonance (Huang *et al* 2009). The results of figure 12 are obtained for tuning at 5000 and 11 000 Hz, and illustrate how the resonant characteristics of the waveguide can be tuned at different frequencies without introducing any physical changes to the structure.

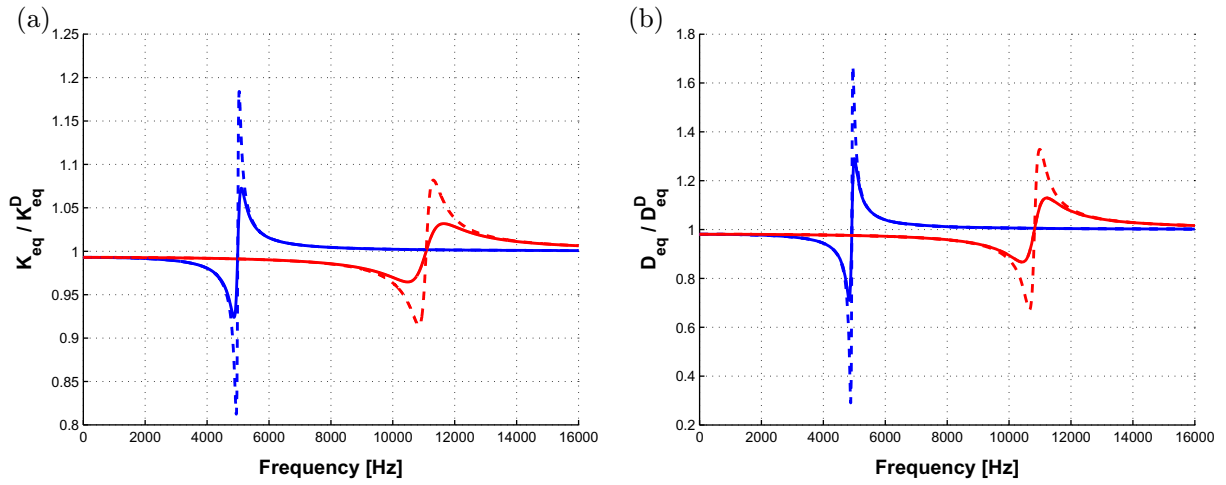


Figure 12. Equivalent axial (a) and bending (b) stiffnesses for different tunings of the piezo shunts (5000 Hz—blue lines; 11 000 Hz—red lines; $R = 25 \Omega$ —solid lines; $R = 50 \Omega$ —dashed lines). Equivalent stiffnesses are normalized with respect to the open circuits values (K_{eq}^D and D_{eq}^D).

The value of resistance R affects the magnitude of the resonance and its frequency bandwidth. High values of resistance correspond to broader ranges of frequencies, and lower amplifications at resonance for the equivalent elastic properties of the beam.

5.3. Dispersion relations

The equivalent properties found through the derivations above are used for the estimation of the dispersion properties of the waveguide. For a beam of equivalent properties given in equation (51), the dispersion relation relating frequency and wavenumber of axial waves is given by the well-known expression (Graff 1975):

$$k_u^{(0)} = \omega \sqrt{\frac{m_{eq}}{K_{eq}}}, \quad (54)$$

where $k_u^{(0)}$ denotes the approximation for $\lambda \gg p$ for the wavenumber of longitudinal waves in the beam. Similarly, the dispersion relation for transverse waves is also given by a well-known expression (Graff 1975):

$$k_w^{(0)} = \left(\omega^2 \frac{m_{eq}}{D_{eq}} \right)^{1/4}, \quad (55)$$

where $k_w^{(0)}$ denotes the approximation for $\lambda \gg p$ for the wavenumber of transverse waves in the beam.

The dispersion relations predicted through the equivalent properties of the beam are compared with the experimental ones visualized through the contour of the magnitude of the 2DFT. Results for the two values of frequency tuning are shown in figure 13. It is interesting to note how the equivalent properties formulation is able to identify the attenuation bands in the approximate ranges of frequency 4850–5150 Hz and 10 500–11 500 Hz. These accurate predictions are obtained in spite of the apparent inconsistency of analytical developments

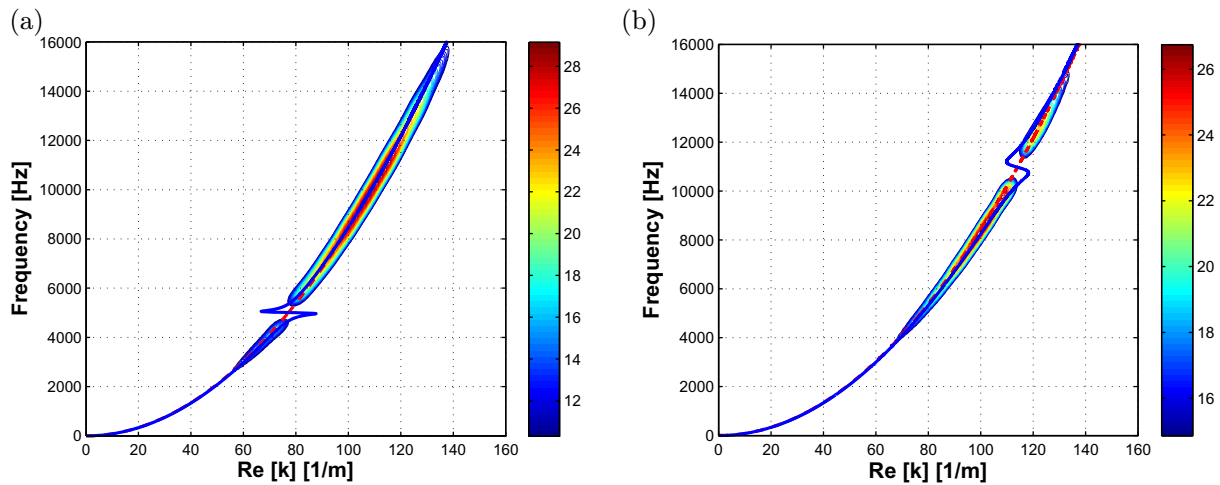


Figure 13. Experimental dispersion relations compared to the analytical predictions from the equivalent properties of the beam: open-circuit—red dashed line; closed-circuit—blue solid line. (a) Tuning at 5000 Hz and $R = 33 \Omega$. (b) Tuning at 11000 Hz and $R = 47 \Omega$.

formulated on the basis of the long-wavelength approximation, and the fact that the periodicity of the beam in this case is such that this assumption does not appear to be valid. However, the considered periodic addition of the piezoelectric patches does not affect the behavior of the beam in terms of added mass and stiffness, at least in the range of frequency considered here, and therefore the selection of a Brillouin zone on the basis of this periodicity appears to be arbitrary and inappropriate. This suggests that for the case at hand, the extension of the equivalent properties estimation for the approximation of the dispersion relations can provide an accurate evaluation of the equivalent properties of the beam, and a good model for the effect of piezoelectric shunting on the equivalent mechanical behavior of the beam.

6. Conclusions

This paper describes the analysis of wave propagation in a periodic beam with shunted piezoelectric patches. The beam is as example of a 1D waveguide connected to a secondary system of periodic resonators. The resonating properties are due to the properties of the shunting circuits, whose impedance can be easily tuned to selected frequency values.

The wave propagation characteristics of the piezoelectric waveguide are first predicted through the application of the TM approach, which is conveniently derived for a structure with piecewise coefficients. The dispersion analysis highlights the occurrence of an internal resonance and the associated generation of an attenuation band at the tuning frequency of the shunts. Such a behavior is found for both axial and bending wave motion. Experimental evidence of the internal resonant behavior of the waveguide is provided through measurements carried out on a beam with a periodic array of 11 patches. The experimental results, analyzed through the application of 1D and 2D FT, effectively confirm the numerical predictions and illustrate the internal resonant characteristics of the waveguide. This behavior is achieved through the multifield coupling between the structural beam and the electrical circuits shunting

the piezo patches. Further insight into the wave mechanics of the waveguide is gained through the development of analytical models of its equivalent mechanical properties. The dispersion relations predicted using this approach illustrate once again the internal resonant behavior of the beam, and capture with good accuracy the trends measured experimentally. The analytical results also suggest that the physical periodicity corresponding to the spacing between the piezo patches may not be an appropriate measure of the periodicity of the waveguide, which effectively behaves as a homogeneous structure with frequency-dependent, resonating mechanical properties.

References

- Behrens S, Moheimani S and Fleming J 2003 *J. Sound Vib.* **266** 929–42
- Casadei F, Ruzzene M, Dozio L and Cunefare K 2010 *Smart Mater. Struct.* **19** 015002
- Cheng Y, Xu J Y and Liu X J 2008 *Phys. Rev. B* **77** 045134
- De Marchi L, Caporale S, Speciale N and Marzani A 2008 *Ultrasonics Symp. 2008 (IUS 2008) IEEE (Piscatawa, NJ)* pp 188–91
- Fang N, Xi D, Xu J, Ambati M, Srituravanich W, Sun C and Zhang X 2006 *Nat. Mater.* **5** 452–56
- Forward R 1979 *J. Appl. Opt.* **18** 690–97
- Gao J, Zou X, Cheng J and Li B 2008 *Appl. Phys. Lett.* **92** 023510
- Graff K 1975 *Wave Motion in Elastic Solids* (New York: Dover)
- Hagood N and von Flotow N 1991 *J. Sound Vib.* **146** 243–68
- Hassani 1998 *Comput. Struct.* **69** 739–56
- Hollkamp J 1994 *J. Intell. Mater. Syst. Struct.* **5** 49–56
- Huang G L and Sun C T 2010 *J. Vib. Acoust.* **132** 031003
- Huang H, Sun C and Huang G 2009 *Int. J. Eng. Sci.* **47** 610–17
- Kushwaha M and Djafari-Rouhani B 1998 *J. Appl. Phys.* **84** 4677–83
- Kushwaha M S, Halevi P, Dobrzynski L and Djafari-Rouhani B 1993 *Phys. Rev. Lett.* **71** 2022–5
- Lazarov B and Jensen J 2007 *Int. J. Non-Linear Mech.* **42** 1186–93
- Lu M, Feng L and Chen Y 2009 *Mater. Today* **12** 34–42
- Martinsson P G and Movchan A B 2003 *Q. J. Mech. Appl. Math.* **56** 45–64
- Ni Q and Cheng J 2005 *Chin. Phys. Lett.* **22** 2305
- Oleinik O 1984 *Lecture Notes in Physics* vol 195, ed P Ciarlet and M Roseau (Berlin: Springer) pp 248–72
- Pai P 2010 *J. Intell. Mater. Syst. Struct.* **21** 517–28
- Preumont A 1997 *Vibration Control of Active Structures* (Dordrecht: Kluwer)
- Riordan R 1967 *Eletron. Lett.* **3** 50–1
- Sheng P, Mei J, Liu Z and Wen W 2007 *Physica B* **394** 256–61
- Sheng P, Zhang X, Liu Z and Chan C 2003 *Physica B* **338** 201–5
- Sigalas M 1998 *J. Appl. Phys.* **84** 3026–30
- Spadoni A, Ruzzene M and Cunefare K 2009 *J. Intell. Mater. Syst. Struct.* **20** 979–90
- Sun H, Du X and Pai P 2010 *J. Intell. Mater. Syst. Struct.* **21** 1085–101
- Thorp O, Ruzzene M and Baz A 2001 *Smart Mater. Struct.* **10** 979–89
- Thorp O, Ruzzene M and Baz A 2005 *Smart Mater. Struct.* **14** 594–604
- Wu S 1996 *Proc. SPIE—The International Society for Optical Engineering* vol 2720 (San Diego, CA) pp 259–69
- Yao S, Zhou X and Hu G 2008 *New J. Phys.* **10** 043020